Warming of southeast Greenland shelf waters in 2016 primes large glacier for runaway retreat

Suzanne L. Bevan[1], Adrian J. Luckman[1], Douglas I. Benn[2], Tom Cowton[2], and Joe Todd[2]

[1]Swansea University, Singleton Park, Swansea SA2 8PP
[2]University of St Andrews, College Gate, St Andrews KY16 9AJ

Correspondence: S. L. Bevan (s.l.bevan@swansea.ac.uk)

Abstract. Kangerdluqssuaq Glacier in southeast Greenland has now retreated further inland than at any time in the past 33 years and its terminus is fast approaching a region of retrograde bedslope, meaning that continued rapid retreat is likely. Here we show that the current retreat was probably driven by anomalously warm surface water on the continental shelf during 2016. The warm surface water likely penetrated the fjord and weakened the mixture of sea ice and icebergs known as mélange, which is normally rigid enough to inhibit calving in winter. The weak mélange allowed Kangerdlugssuaq Glacier to calve throughout the winters of 2016/17 and 2017/18 preventing the regular seasonal advance. As calving continued uninterruptedly from summer 2016 to the end of 2018 the glacier accelerated by 35% and thinned by 35 m. These observations demonstrate the importance of near-surface ocean temperatures on tidewater glacier stability, and remind us that it is not only deep-ocean warming that can lead to glacier retreat.

1 Introduction

Since the early 1990s the Greenland Ice Sheet (GrIS) has been a major contributor to sea-level rise, losing a total of 2700±930 Gt of ice between 1992 and 2011 (Shepherd et al., 2012). About 40% of the 0.47±0.23 mm/year mean 1991–2015 sea-level rise originating from Greenland was caused by increases in the rate at which glaciers calve ice into the oceans, and the remainder by increases in surface melt and runoff (van den Broeke et al., 2016). Kangerdlugssuaq Glacier (KG) is a large tidewater-terminating glacier in southeast Greenland (Fig. 1) which delivers around 24 Gt/year of ice to the ocean, equivalent to about 5% of GrIS total discharge (Enderlin et al., 2014). In 2004 the calving front of KG suddenly retreated by over 6 km, its surface flow speeds doubled (Howat et al., 2005; Luckman et al., 2006), and between 2003 and 2007 the glacier thinned by over 100 m (Khan et al., 2014). The rapid retreat of KG was accompanied by a similar pattern of change in many other southeast Greenland outlet glaciers and accounted for ∼16% of the total 2000–2005 net mass loss of the GrIS (Rignot and Kanagaratnam, 2006). KG thus typifies the response of Greenland outlet glaciers to climate forcing whilst being an individually important source of sea level rise. After 2006, KG slowed down, although speeds remained at least 20% greater than pre-retreat values, and the ice front maintained a steady mean annual position, with seasonal advances and retreats of up to 6 km (Kehrl et al., 2017).

The synchronous retreat of southeast Greenland glaciers in the early 2000s suggested that atmospheric and/or ocean warming were responsible for initiating the rapid retreat, thinning and subsequent dynamic response (Howat et al., 2008; Hanna et al., 2009; Murray et al., 2010; Howat and Eddy, 2011; Christoffersen et al., 2011; Inall et al., 2014). Nevertheless, local differences in glacier and fjord geometry, and connection to the ocean normally determine individual responses to changing environmental conditions (Moon et al., 2012; Enderlin et al., 2013; Millan et al., 2018). When KG retreated in 2004 it did so into deeper water (Khan et al., 2014) — such a reverse or retrograde bed slope can set up a positive feedback between frontal retreat, ice discharge and dynamic thinning (Schoof, 2007). KG's retreat was halted in mid 2011 only when its grounding line once again reached shallower water. At that stage thinning had slowed, the final few km of the glacier was afloat (Khan et al., 2014; Kehrl et al., 2017), and there was a balance between advance of the calving front in winter and its retreat in summer.

KG calves into the head of a 75 km long, 5–10 km wide, fjord (Murray et al., 2010; Sutherland et al., 2014) (KF); the fjord has a wide mouth and is connected to the shelf break by a deep, straight, 300 km long trough (Dowdeswell et al., 2010; Inall et al., 2014). Much of the passage from ocean to glacier is 600–900 m deep with sills shallowing to 400–550 m at the fjord mouth and within the shelf trough (Fig. 1). The increase in mass loss from the southeast GrIS to the ocean that began in the mid 1990s coincided with a warming of the North Atlantic Ocean (Straneo and Heimbach, 2013) and the relatively unimpeded connection of KG with the ocean was shown to have allowed increasing ocean temperatures to trigger retreat in 2004 (Christoffersen et al., 2011; Inall et al., 2014; Jackson et al., 2014; Millan et al., 2018).

Here we show that by the end of 2018, following two winters when KG unusually failed to advance, its calving front was further retreated than at any point in the satellite record (33 years). We present evidence that recent retreat was triggered by the weakening of ice mélange in the fjord, a mechanism only previously shown by association (Moon et al., 2015). We propose that the mélange weakening is explained by exceptionally warm surface waters originating from outside the fjord. The observed contemporaneous interannual thinning superimposed on the seasonal cycle of surface elevation change will leave the glacier vulnerable to basal melt and further rapid retreat.

2 Methodology and Data

2.1 Frontal positions

Glacier fronts were manually digitised on a variety of optical and synthetic aperture radar (SAR) satellite images. We located the intersection points of the digitised fronts with a series of parallel linear flowlines at 160 m spacing, and the frontal change was calculated by taking the mean of the changes in these intersection points (Luckman et al., 2015). From 1985–2012 the images include Landsat-5 (TM Band 4) and Landsat-7 (ETM+ Band 8), European Remote Sensing satellites (ERS-1 and ERS-2), and Envisat Advanced Synthetic Aperture Radar (ASAR) Image (IM) and Wideswath mode (WSM) data (Bevan et al., 2012). From 2011–2018 we use TerraSAR-X SAR data, and additionally, from 2015–2019, Sentinel 1A and 1B Ground Range Detected High-resolution Interferometric Wideswath (GRDH, IW) images. Image spatial resolution ranges from 30 m for Landsat-5 to 8 m for the multi-looked TerraSAR-X data. All images were reprojected to the Polar Stereographic co-ordinate system before the fronts were digitised. Appendix Fig. A1 shows which observations derived from which satellite missions.

2.2 Surface velocities

Surface velocities were derived using feature tracking — see Bevan et al. (2012) for details of the early (1985–2012) part of the time series. After 2011 velocities are based on TerraSAR-X SAR and Sentinel 1A and 1B single-look complex (SLC) data using Gamma Remote Sensing software. Pairs of TerraSAR-X SLCs with 11 day time separation were tracked using a window spacing of 40 m and the results converted to ground range and geocoded using coincident interferometric DEMs (Section 2.4). Sentinel-1 pairs were tracked with pair delays of either 6 or 12 days, with a window spacing of 100 m and geocoded using the 90 m Greenland Icesheet Mapping Project (GIMP) DEM (Howat et al., 2014). Appendix Fig. A1 shows which velocity measurements derived from which satellite missions.

2.3 Ocean and surface air temperatures

Ocean potential temperatures for 1991–2017 were extracted from Arctic Ocean Physics Reanalysis monthly mean data supplied by the Copernicus Marine Environment Monitoring Service (CMEMS). Temperatures for 2018 were based on monthly means of the Arctic Ocean Analysis and Forecast Product (also supplied by CMEMS) which are available at daily intervals. Both the reanalysis and the analysis/forecast products are based on a 3D physical ocean and sea-ice model that assimilates remotely sensed and in-situ data, and have a spatial resolution of 12.5 km, and 12 depth levels distributed unevenly between 5 and 3000 m. We plot mean 5 m temperatures and anomalies over the Kangerdlugssuaq trough area. Temperatures from published Conductivity Temperature Depth (CTD) profiles are used to compare fjord temperatures in 2017 with earlier years.

Air temperatures at 2 m were extracted from the Danish Meteorological Institute weather reports for Aputiteeq (station number 04351) at the entrance to KF, and Tasiilaq (station number 04360, see Fig. 1). Anomalies in monthly mean 1200 UTC 2 m air temperatures were calculated relative to the period 1987–2018; 1987 being the first year for observations at Aputiteeq. When data were missing for Aputiteeq we substituted with data from the nearest alternative station Tasiilaq (station number 04360) 342 km to the south at the entrance to Sermilik Fjord.

2.4 Surface elevation

A time series of 150 Digital Elevation Models (DEMs) from June 2011 to July 2018 were created using experimental SAR data from the TanDEM-X satellite system which comprises the TerraSAR-X and TerraSAR-X add on for Digital Elevation Measurement (TanDEM-X) satellites. We used Gamma Remote Sensing software to interfere, unwrap and geocode the bistatic stripmap mode Co-registered Single look Slant range Complex images (CoSSCs). The CoSSCs have a spatial resolution of $\sim$2 m and the DEMs were smoothed to a horizontal resolution of 8 m. We used the provided orbital vector data and the 30 m GIMP DEM (Howat et al., 2014) to initially geolocate and phase scale the images; geolocation was iteratively improved using the interferometrically generated DEMs. The interferograms were unwrapped from a bare-rock location on the south side of the glacier (33.0365°W,68.5939°N), and the DEMs tied in the vertical to this point using the GIMP DEM height (730 m). Only CoSSCs with satellite separations perpendicular to the look direction of less than 500 m were used because longer baselines prevented satisfactory unwrapping. This restriction meant that there were fewer DEMs created for 2015. Elevations

are given relative to the WGS84 reference ellipsoid. Orbit uncertainties (Krieger et al., 2013) mean that we cannot expect relative elevation accuracies better than 2 m. The standard deviation of DEM heights at a point on the opposite side of the fjord to the unwrapping start point was 2.3 m, indicating that unwrapping errors were minimised even across the glacier. The accuracy of absolute height values depends on the accuracy of, and geolocation with respect to the GIMP DEM. The GIMP DEM in turn is quoted as having a vertical precision of between ± 1.0 m over most ice areas and ± 30 m over areas of high relief (Howat et al., 2014). We therefore estimate absolute errors of the order of ± 10 m which is the root mean squared validation error of the GIMP DEM with respect to ICESat.

We used IceBridge BedMachine Greenland, Version 3 data (Morlighem et al., 2017) together with the hydrostatic equilibrium assumption to determine where the glacier surface was above flotation height. We used an ice density of 917 kg/m^3, and a sea-water density of 1023 kg/m^3. At the location of KG, WGS84 datum is 55 m below the Geoid.

3 Results and Discussion

3.1 Interruption of normal winter advance in 2017 and 2018

Our long and detailed record of ice-front position shows that before the 2004 retreat and from 2005 to the end of 2016, KG maintained a relatively stable mean-annual frontal position (Fig. 2). The clear seasonal variation in ice-front position is characterised by an advance of 2 to 6 km from January until July or August (which we will refer to simply as winter), with almost no calving events. During the second half of the year (summer) the front normally retreats in a similar steady manner. By contrast, in 2017 and 2018, the glacier continued to calve throughout both summer and winter, only advancing a fraction of the normal distance between the beginning of January and the end of July in 2017, and not at all in 2018 (Fig. 3a). This lack of sustained winter advance has only occurred twice before in the observed record: 1996, and 2005 which marked the previous episode of retreat and thinning (Fig. 2, Luckman et al., 2006). By the start of summer 2018 the ice front had retreated by 8 km relative to the start of summer 2016 and the anomalous winter calving continued into the summer months.

The winter advance of KG coincides with the formation of a rigid mélange consisting of icebergs bound together with sea ice. Although interstitial sea ice likely contributes little to mélange strength, it prevents iceberg dispersal and thus encourages the transfer of back stress from the fjord sides to the glacier front via compressional stress bridges between adjacent icebergs (Burton et al., 2018). Such stress bridges are not commonly visible on satellite imagery, because 90% of iceberg mass is below the waterline. However, surface features in the mélange can betray the existence of back stress. Figure 5 shows a TerraSAR-X image from 30 March 2016, when the mélange was frozen into a coherent mass. A series of transverse ridges in the mélange on the up-fjord side of a large promontory shows that it was under compression, confirming the presence of back stress on the glacier front. This promontory appears to provide a critical component of the back stress at KG; up-fjord of the promontory, the mélange shears past landfast ice along a narrow shear zone, while down-fjord, the mélange is typically not in contact with the northern fjord margin. Back stress from mélange is clearly insufficient to resist advance of the glacier front, but it inhibits calving by reducing crevasse propagation and preventing the detachment of icebergs, even where the ice is heavily fractured.

It has been demonstrated theoretically that the amount of back stress necessary to prevent calving is of the order of 10^7 N/m and that this can be supplied by ice mélange (Amundson et al., 2010; Krug et al., 2015).

At KG the mélange normally inhibits detachment of icebergs from the glacier front until sea ice melts and the mélange disperses with the onset of summer — resulting in the seasonal advance/retreat cycle. Modelling studies have shown that the inhibiting effect of ice mélange on calving is capable of generating much larger (km scale) seasonal advance and retreat cycles than the annual variation in submarine frontal melt (Todd and Christoffersen, 2014; Krug et al., 2015).

In contrast to previous years, in early 2017 and 2018, formation of a rigid mélange was repeatedly interrupted by episodes of break-up and dispersal. Close examination of a series of synthetic aperture radar (SAR) images from Sentinel 1 reveals that each mélange breakup episode commenced at the down-fjord edge and propagated towards the glacier front, culminating in large calving events (Fig. 4, and Video 1). In consequence, the normal sustained advance during winter was punctuated by several periods of calving. This behaviour is similar to that usually experienced in the autumn and early winter, when rigid mélange repeatedly forms and breaks up. The failure of KG to advance in the winters of 2017 and 2018 could thus reflect weakly bonded mélange and indicates that conditions in the fjord were not conducive to the formation of mélange at this time.

3.2 Atmospheric and Oceanic conditions

Our observations strongly suggest that the onset of retreat at KG in 2016 was caused by a weakened ice mélange, facilitating winter calving and thus preventing the usual winter advance of the terminus. The overarching cause of retreat may therefore lie in a warming of air temperatures, ocean temperatures, or a combination of these effects.

3.2.1 Air temperature

Mild air temperatures, particularly during the winter months, could contribute to weakened ice mélange by delaying or limiting sea ice formation. Conditions were anomalously warm throughout 2016 relative to the 1987–2018 mean, most notably between September 2016 and February 2017 (Fig. 3b). Similarly, exceptionally mild air temperatures were recorded between December and April of the following winter. It therefore seems probable that mild winter air temperatures played an important role in weakening the ice mélange and driving retreat at KG. It is, however, notable that exceptionally warm air temperatures (up to 6°C above the 1987–2018 mean) were also recorded between January and April 2014, but without any apparent impact on the winter advance of KG on this occasion. It may therefore be that warm winter air temperatures alone are not necessarily sufficient to inhibit mélange formation without favourable ocean conditions.

3.2.2 Ocean temperature

In 2016 the surface waters on the southeast Greenland continental shelf were exceptionally warm: by July and August 2016 potential temperatures at a depth of 5 m were up to 4°C warmer than the 1992–2018 mean (Appendix, Fig. A2) and the anomalies persisted into the first half of 2017 (Fig. 3b). This warming in part reflects the high regional air temperatures during this time, but was also driven by an increased advection of water from the Atlantic Ocean (Timmermans , 2016).

If these exceptionally warm surface waters were able to propagate into the fjord, then they may have contributed significantly towards the weakened ice mélange at KG during winter 2016/17. Although there is no record of water properties within KF in 2016, observations from previous years (Inall et al., 2014; Sutherland et al., 2014), and numerical modelling experiments (Cowton et al., 2016), indicate that seasonally warmed shelf surface waters (termed Polar Surface Water warm, PSWw) can readily penetrate far into KF. These studies reveal the prevalence of a complex, multi-layered circulation in KF during the summer melt season. Turbulent upwelling, forced by the input of meltwater at the glacier termini (and in particular KG), creates an outflowing tongue of relatively cool glacially modified waters (GMW) at a depth of $\sim$100 m, with a compensatory up-fjord flow of warm, salty Atlantic waters (AW) below this. Above the GMW, circulation is characterised by a secondary cell in which PSWw is drawn towards the fjord head, capped by a thin ($\sim$10 m) layer of outflowing cool, fresh water. Numerical modelling (Cowton et al., 2016), and analysis of these waters in temperature–salinity space (Inall et al., 2014), indicate that this surface outflow is forced by the input of freshwater from surface runoff and shallow tidewater glaciers. The upper cell therefore resembles a classic estuarine circulation, with the up-fjord flow of PSWw driven by turbulent mixing at the interface between these overlying layers.

Observations show that PSWw may constitute the warmest water mass in KF during the summer months (Inall et al., 2014). Although it experiences cooling through mixing and iceberg melt during up-fjord transit, available hydrographic data from the inner fjord demonstrate it remains relatively warm ($\sim 0.5 - 1.5^{\circ}$C) even at this distance from the shelf (Fig. 6). Thus, while considerable attention has been given to AW as a driver of submarine melting (Straneo and Heimbach, 2013), PSWw represents an important yet comparatively overlooked component of the fjord heat budget. Inall et al. (2014) calculated that PSWw accounts for 25% of ice melt within the fjord system reflecting its warmth and proximity to floating ice within the fjord. Indeed, its location near the fjord surface means that it could inhibit mélange formation. We therefore believe that exceptionally warm PSWw played an important role in the weakening of the ice mélange, and thus onset of retreat, at KG in 2016/17.

In addition to the anomalously warm shelf surface waters, it is possible that a warming of subsurface AW may have contributed to the retreat of KG. Reanalysis data suggest that subsurface waters in Kangerdlugssuaq trough warmed steadily since the early 2010s to reach a high during 2016–2018. Facilitated by an absence of shallow sills, these subsurface waters are advected into KF by both the buoyancy-driven circulation described above and by coastally trapped waves associated with winter storms (Jackson et al., 2014; Cowton et al., 2016; Fraser and Inall, 2018). The retreat of KG and other Greenlandic tidewater glaciers has been associated with a warming of coastal AW (Straneo and Heimbach, 2013; Cowton et al., 2018), although the difficulty of observing frontal processes at tidewater glaciers means that a causal link has proven difficult to confirm.

While warming AW may have helped precondition KG for retreat, there are several reasons why we believe it is unlikely to have been the principal cause of the retreat commencing in 2016. Firstly, the onset of retreat in winter, and observations of reduced mélange rigidity immediately prior to calving, indicate that the retreat was triggered by a weakening of the mélange, most likely due to reduced sea ice formation. While the subsurface input of meltwater at KG drives vigorous upwelling of AW, observations and modelling indicate that this reaches neutral buoyancy and flows out of the fjord at depths greater than $\sim$50m (Inall et al., 2014; Cowton et al., 2016). At these depths it may contribute to melting of larger icebergs in the mélange, but will have little impact on sea ice formation at the fjord surface. Secondly, while reanalysis data indicates that AW in

Kangerdlugssuaq trough has warmed in recent years, this warming has been relatively gradual, with no obvious trigger for retreat in 2016/17. This contrasts with surface waters, which experienced record-breaking temperatures in 2016. Thirdly, a hydrographic profile obtained from KF during autumn 2017 does not show particularly warm AW in the fjord at this time (Fig. 6). This implies that the apparent warming of trough waters may to some extent be an artefact of the reanalysis data, or may not be effectively translated into an actual warming of AW in KF.

We therefore propose that the exceptionally warm surface waters on the east Greenland shelf during 2016 and early 2017, and consequently the presence of anomalously warm PSWw within KF, played a critical role in triggering the recent retreat of KG. Combined with mild air temperatures, we suggest these warm, near-surface waters will have acted to delay and weaken winter sea ice formation, reducing mélange rigidity and thus allowing increased winter calving of KG. The possibility that anomalously warm PSWw could be responsible for episodes of retreat at KG has been previously hypothesised; Christoffersen et al. (2011) noted that CTD data from inner KF showed PSWw at $> 2°$C shortly prior to the major retreat of 2004, compared with $< -1°$C during a previous survey during the stable year of 1993. Similarly, warm anomalies were reported in PSWw (based on sea surface temperatures (SSTs) at the fjord mouth) in 2004 and 2010 (Inall et al., 2014), both years with winter calving of KG. With the improved resolution and frequency of available remote sensing imagery, we are able to provide further evidence that weakness in the mélange, following a year of exceptional near-surface ocean temperatures, can cause reduced winter advance of KG.

A question remains as to the cause of the continued retreat during 2017/18, a period during which shelf surface waters were not observed to be anomalously warm although air temperatures in early 2018 were almost 6° above average. It is possible that the ongoing retreat is a dynamical consequence of the retreat commencing in 2016/17, with the glacier entering a phase of self-sustaining instability (Joughin et al., 2008).

3.3 Implications of further retreat

A decrease in surface elevations of outlet glaciers in the early 1990s was one of the first indications that the GrIS was losing mass via increased surface melt and dynamic thinning (Krabill et al., 2000; Krabill, 2004). Dynamic thinning is the result of acceleration when retreat and melt-driven thinning reduce resistive stresses at the glacier front. Seasonal cycles of dynamic thinning have recently been observed on Helheim, another large tidewater glacier 300 km to the south of KG (Bevan et al., 2015), where they are associated with fluctuations in ice-front position (Kehrl et al., 2017).

We also see dynamic thinning on KG. The high temporal resolution time series of velocities for KG (Fig. 3a) shows a summer acceleration as the ice-front retreats and winter slowdown as it advances. Associated with this seasonal velocity pattern is a seasonal dynamic change in KG surface elevations — the glacier thins as it retreats and accelerates, and thickens as it advances and slows (Figs. 3a and c).

At the start of 2017, when the normal winter advance faltered, velocities increased and the acceleration was sustained through to summer 2018, by which time KG was flowing 35% faster than two years earlier (Fig. 3a). During this period (June 2016 to May 2018) a thinning of 35 m, caused by the increase in velocity, is superimposed on the seasonal thinning (Figs. 3c and Fig. 8). Surface elevations relative to sea-level and an assumption of hydrostatic equilibrium indicate that in summer 2016 the

final 5 km of the glacier was floating; the velocity profile (Fig. 8, for 04/06/2014, when the glacier thickness and front location were similar to summer 2016) confirms this. The reduction in down-flow acceleration between kilometers 11 and 4 is consistent with transition to a floating tongue and loss of basal drag. By May 2018 (the last available DEM) most of this floating tongue had been lost and the ice front was left only 1 km ahead of the start of a section of reverse bed slope (Figs. 7 and 8).

The two-year retreat of KG to a point only a kilometre or so ahead of the reverse bedrock slope, and further up fjord than at any point in the observation record, has placed the glacier in a precarious position. Continued dynamic thinning as it retreats and accelerates is likely to result in the ice front refloating when it will then be susceptible to basal melt and further thinning. KG may only stabilise where the prograde bed slope is reached some 6 km upstream.

4 Conclusions

We conclude that the retreat of KG in 2017 and 2018 was driven by anomalously warm water on the shelf in the latter half of 2016 which likely penetrated the fjord. Our observations reveal a weakened winter ice mélange in 2017 and 2018 that allowed sustained calving when the glacier would normally be advancing. Any additional retreat of KG will take the terminus into a region of retrograde bed slope, which could result in further retreat and thinning via dynamics and basal melt.

Our research emphasises the importance of accounting for the delivery of heat into the fjords of Greenland by surface as well as deep water. Heat delivered by surface water can weaken the stabilizing influence of ice mélange proximal to ocean-terminating glaciers, disrupting the seasonal calving pattern and triggering terminus retreat.

Data availability. The NERC Polar Data Centre hosts the timeseries data on frontal positions (https://doi.org/10.5285/b317f707-2ef6-449c-acc3-6bb087efecb1), surface velocities (https://doi.org/10.5285/c26e3873-e33e-45be-b76b-87f3b8827101) and surface elevations (https://doi.org/10.5285/3bbacca6-d2cd-46be-b824-b828572ca486), and Video 1 (https://doi.org/10.5285/61100705-dfbc-489d-b729-1268ec743bbf).

Author contributions. The study was led and the manuscript drafted by Suzanne Bevan, the project was led by Doug Benn and Adrian Luckman. Expert advice, data and contributions to the text and figures were supplied by Adrian Luckman (SAR imagery and glacier velocities), Douglas Benn and Joe Todd (interpretation of glacier calving and interaction with mélange), Tom Cowton (fjord processes). TanDEM-X DEMs were processed by Suzanne Bevan.

Competing interests. The authors declare that they have no competing interests.

Acknowledgements. The research under project CALISMO (Calving Laws for Ice Sheet Models) was funded by the Natural Environment Research Council (NERC) grants NE/P011365/1. TanDEM-X data used for generating the DEMs and for ice-front positions and glacier velocities were supplied by DLR, as part of NERC project NE/I0071481/1. Satellite imagery for front positions were supplied by European Space Agency (ERS-1 and -2, Envisat, Sentinel), the U.S. Geological Survey (Landsat). BedMachine data were obtained from NASA National Snow and Ice Data Center Distributed Active Archive Center. doi: https://doi.org/10.5067/2CIX82HUV88Y. [16/01/2018]. DMI weather observations were downloaded from www.dmi.dk/publikationer. The CMEMS ocean reanalysis data was downloaded from ftp://mftp.cmems.met.no/Core/ARCTIC_REANALYSIS_PHYS_002_003/dataset-ran-arc-myoceanv2-be, and the ocean analysis and forecast data from ftp://mftp.cmems.met.no/Core/ARCTIC_ANALYSIS_FORECAST_PHYS_002_001_a/dataset-topaz4-arc-myoceanv2-be.

References

Amundson, J. M., Fahnestock, M., Truffer, M., Brown, J., Lüthi, M. P., and Motyka, R. J.: Ice mélange dynamics and implications for terminus stability, Jakobshavn Isbræ, Greenland, Journal of Geophysical Research, 115, F01 005+, https://doi.org/10.1029/2009jf001405, 2010.

Andrews, J. T., Milliman, J. D., Jennings, A. E., Rynes, N., and Dwyer, J.: Sediment Thicknesses and Holocene Glacial Marine Sedimentation Rates in Three East Greenland Fjords (ca. 68°N), The Journal of Geology, 102, 669–683, https://doi.org/10.1086/629711, 1994.

Azetsu-Scott, K. and Syvitski, J. P. M.: Influence of melting icebergs on distribution, characteristics and transport of marine particles in an East Greenland fjord, Journal of Geophysical Research: Oceans, 104, 5321–5328, https://doi.org/10.1029/1998jc900083, 1999.

Bevan, S. L., Luckman, A. J., and Murray, T.: Glacier dynamics over the last quarter of a century at Helheim, Kangerdlugssuaq and 14 other major Greenland outlet glaciers, The Cryosphere, 6, 923–937, https://doi.org/10.5194/tc-6-923-2012, 2012.

Bevan, S. L., Luckman, A., Khan, S. A., and Murray, T.: Seasonal dynamic thinning at Helheim Glacier, Earth and Planetary Science Letters, 415, 47–53, https://doi.org/10.1016/j.epsl.2015.01.031, 2015.

Burton, J. C., Amundson, J. M., Cassotto, R., Kuo, C.-C. C., and Dennin, M.: Quantifying flow and stress in ice mélange, the world's largest granular material., Proceedings of the National Academy of Sciences of the United States of America, 115, 5105–5110, http://view.ncbi.nlm.nih.gov/pubmed/29712869, 2018.

Christoffersen, P., Mugford, R. I., Heywood, K. J., Joughin, I., Dowdeswell, J. A., Syvitski, J. P. M., Luckman, A., and Benham, T. J.: Warming of waters in an East Greenland fjord prior to glacier retreat: mechanisms and connection to large-scale atmospheric conditions, The Cryosphere, 5, 701–714, https://doi.org/10.5194/tc-5-701-2011, 2011.

Cowton, T., Sole, A., Nienow, P., Slater, D., Wilton, D., and Hanna, E.: Controls on the transport of oceanic heat to Kangerdlugssuaq Glacier, East Greenland, Journal of Glaciology, 62, 1167–1180, https://doi.org/10.1017/jog.2016.117, 2016.

Cowton, T. R., Sole, A. J., Nienow, P. W., Slater, D. A., and Christoffersen, P.: Linear response of east Greenland's tidewater glaciers to ocean/atmosphere warming, Proceedings of the National Academy of Sciences, 115, 7907–7912, https://doi.org/10.1073/pnas.1801769115, 2018.

Dowdeswell, J.: Cruise report - JR106b. RSS James Clark Ross. Kangerdlugssuaq Fjord and shelf, east Greenland. NERC Autosub Under Ice thematic programme, 2004

Dowdeswell, J. A., Evans, J., and Cofaigh: Submarine landforms and shallow acoustic stratigraphy of a 400 km-long fjord-shelf-slope transect, Kangerlussuaq margin, East Greenland, Quaternary Science Reviews, 29, 3359–3369, https://doi.org/10.1016/j.quascirev.2010.06.006, 2010.

Enderlin, E. M., Howat, I. M., and Vieli, A.: High sensitivity of tidewater outlet glacier dynamics to shape, The Cryosphere, 7, 1007–1015, https://doi.org/10.5194/tc-7-1007-2013, 2013.

Enderlin, E. M., Howat, I. M., Jeong, S., Noh, M.-J., van Angelen, J. H., and van den Broeke, M. R.: An improved mass budget for the Greenland ice sheet, Geophysical Research Letters, 41, 2013GL059 010+, https://doi.org/10.1002/2013gl059010, 2014.

Fraser, N. J. and Inall, M. E.: Influence of Barrier Wind Forcing on Heat Delivery Towards the Greenland Ice Sheet, Journal of Geophysical Research: Oceans, https://doi.org/10.1002/2017jc013464, 2018.

Hanna, E., Cappelen, J., Fettweis, X., Huybrechts, P., Luckman, A., and Ribergaard, M. H.: Hydrologic response of the Greenland ice sheet: the role of oceanographic warming, Hydrological Processes, 23, 7–30, https://doi.org/10.1002/hyp.7090, 2009.

Howat, I. M. and Eddy, A.: Multi-decadal retreat of Greenland's marine-terminating glaciers, Journal of Glaciology, pp. 389–396, https://doi.org/10.3189/002214311796905631, 2011.

Howat, I. M., Joughin, I., Tulaczyk, S., and Gogineni, S.: Rapid retreat and acceleration of Helheim Glacier, east Greenland, Geophysical Research Letters, 32, L22 502+, https://doi.org/10.1029/2005gl024737, 2005.

Howat, I. M., Joughin, I., Fahnestock, M., Smith, B. E., and Scambos, T. A.: Synchronous retreat and acceleration of southeast Greenland outlet glaciers 2000–06: ice dynamics and coupling to climate, Journal of Glaciology, 54, 646–660, https://doi.org/10.3189/002214308786570908, 2008.

Howat, I. M., Box, J. E., Ahn, Y., Herrington, A., and McFadden, E. M.: Seasonal variability in the dynamics of marine-terminating outlet glaciers in Greenland, Journal of Glaciology, 56(198), 601–613, https://doi.org/10.3189/002214310793146232, 2010.

Howat, I. M., Negrete, A., and Smith, B. E.: The Greenland Ice Mapping Project (GIMP) land classification and surface elevation data sets, The Cryosphere, 8, 1509–1518, https://doi.org/10.5194/tc-8-1509-2014, 2014.

Inall, M. E., Murray, T., Cottier, F. R., Scharrer, K., Boyd, T. J., Heywood, K. J., and Bevan, S. L.: Oceanic heat delivery via Kangerdlugssuaq Fjord to the south-east Greenland ice sheet, Journal of Geophysical Research: Oceans, 119, 631–645, https://doi.org/10.1002/2013jc009295, 2014.

Jackson, R. H., Straneo, F., and Sutherland, D. A.: Externally forced fluctuations in ocean temperature at Greenland glaciers in non-summer months, Nature Geoscience, 7, 503–508, https://doi.org/10.1038/ngeo2186, 2014.

Jakobsson, M., Mayer, L., Coakley, B., Dowdeswell, J. A., Forbes, S., Fridman, B., Hodnesdal, H., Noormets, R., Pedersen, R., Rebesco, M., Schenke, H. W., Zarayskaya, Y., Accettella, D., Armstrong, A., Anderson, R. M., Bienhoff, P., Camerlenghi, A., Church, I., Edwards, M., Gardner, J. V., Hall, J. K., Hell, B., Hestvik, O., Kristoffersen, Y., Marcussen, C., Mohammad, R., Mosher, D., Nghiem, S. V., Pedrosa, M. T., Travaglini, P. G., and Weatherall, P.: The International Bathymetric Chart of the Arctic Ocean (IBCAO) Version 3.0, Geophysical Research Letters, 39, n/a, https://doi.org/10.1029/2012gl052219, 2012.

Joughin, I., Howat, I. M., Fahnestock, M., Smith, B., Krabill, W., Alley, R. B., Stern, H., and Truffer, M.: Continued evolution of Jakobshavn Isbrae following its rapid speedup, Journal of Geophysical Research, 113, F04 006+, https://doi.org/10.1029/2008jf001023, 2008.

Kehrl, L. M., Joughin, I., Shean, D. E., Floricioiu, D., and Krieger, L.: Seasonal and interannual variabilities in terminus position, glacier velocity, and surface elevation at Helheim and Kangerlussuaq Glaciers from 2008 to 2016, Journal of Geophysical Research: Earth Surface, pp. 2016JF004 133+, https://doi.org/10.1002/2016jf004133, 2017.

Khan, S. A., Kjeldsen, K. K., Kjær, K. H., Bevan, S., Luckman, A., Aschwanden, A., Bjørk, A. A., Korsgaard, N. J., Box, J. E., van den Broeke, M., van Dam, T. M., and Fitzner, A.: Glacier dynamics at Helheim and Kangerdlugssuaq glaciers, southeast Greenland, since the Little Ice Age, The Cryosphere, 8, 1497–1507, https://doi.org/10.5194/tc-8-1497-2014, 2014.

Krabill, W.: Greenland Ice Sheet: Increased coastal thinning, Geophysical Research Letters, 31, 194+, https://doi.org/10.1029/2004gl021533, 2004.

Krabill, W., Abdalati, W., Frederick, E., Manizade, S., Martin, C., Sonntag, J., Swift, R., Thomas, R., Wright, W., and Yungel, J.: Greenland ice sheet: High-elevation balance and peripheral thinning, Science, 289, 428–430, 2000.

Krieger, G., Zink, M., Bachmann, M., Bräutigam, B., Schulze, D., Martone, M., Rizzoli, P., Steinbrecher, U., Walter Antony, J., De Zan, F., Hajnsek, I., Papathanassiou, K., Kugler, F., Rodriguez Cassola, M., Younis, M., Baumgartner, S., López-Dekker, P., Prats, P., and Moreira, A.: TanDEM-X: A radar interferometer with two formation-flying satellites, Acta Astronautica, 89, 83–98, https://doi.org/10.1016/j.actaastro.2013.03.008, 2013.

Krug, J., Durand, G., Gagliardini, O., and Weiss, J.: Modelling the impact of submarine frontal melting and ice mélange on glacier dynamics, The Cryosphere, 9, 989–1003, https://doi.org/10.5194/tc-9-989-2015, 2015.

Luckman, A., Murray, T., de Lange, R., and Hanna, E.: Rapid and synchronous ice-dynamic changes in East Greenland, Geophysical Research Letters, 33, 33 729+, https://doi.org/10.1029/2005gl025428, 2006.

Luckman, A., Benn, D. I., Cottier, F., Bevan, S., Nilsen, F., and Inall, M.: Calving rates at tidewater glaciers vary strongly with ocean temperature, Nature Communications, 6, 8566+, https://doi.org/10.1038/ncomms9566, 2015.

Millan, R., Rignot, E., Mouginot, J., Wood, M., Bjørk, A. A., and Morlighem, M.: Vulnerability of Southeast Greenland Glaciers to Warm Atlantic Water From Operation IceBridge and Ocean Melting Greenland Data, Geophysical Research Letters, https://doi.org/10.1002/2017gl076561, 2018.

Moon, T., Joughin, I., Smith, B., and Howat, I.: 21st-Century Evolution of Greenland Outlet Glacier Velocities, Science, 336, 576–578, https://doi.org/10.1126/science.1219985, 2012.

Moon, T., Joughin, I., and Smith, B.: Seasonal to multiyear variability of glacier surface velocity, terminus position, and sea ice/ice mélange in northwest Greenland: NW GLACIER VARIABILITY, Journal of Geophysical Research: Earth Surface, 120, 818–833, https://doi.org/10.1002/2015jf003494, 2015.

Morlighem, M., Williams, C. N., Rignot, E., An, L., Arndt, J. E., Bamber, J. L., Catania, G., Chauché, N., Dowdeswell, J. A., Dorschel, B., Fenty, I., Hogan, K., Howat, I., Hubbard, A., Jakobsson, M., Jordan, T. M., Kjeldsen, K. K., Millan, R., Mayer, L., Mouginot, J., Noël, B. P. Y., O'Cofaigh, C., Palmer, S., Rysgaard, S., Seroussi, H., Siegert, M. J., Slabon, P., Straneo, F., van den Broeke, M. R., Weinrebe, W., Wood, M., and Zinglersen, K. B.: BedMachine v3: Complete Bed Topography and Ocean Bathymetry Mapping of Greenland From Multibeam Echo Sounding Combined With Mass Conservation, Geophysical Research Letters, 44, 2017GL074 954+, https://doi.org/10.1002/2017gl074954, 2017.

Murray, T., Scharrer, K., James, T. D., Dye, S. R., Hanna, E., Booth, A. D., Selmes, N., Luckman, A., Hughes, A. L. C., Cook, S., and Huybrechts, P.: Ocean regulation hypothesis for glacier dynamics in southeast Greenland and implications for ice sheet mass changes, Journal of Geophysical Research, 115, doi:10.1029/2009JF001 522+, https://doi.org/10.1029/2009jf001522, 2010.

OMG Mission (2016).: Conductivity, Temperature and Depth (CTD) data from the ocean survey. Ver. 0.1. OMG SDS, CA, USA. http://dx.doi.org/10.5067/OMGEV-AXCTD, 2018.

Rignot, E. and Kanagaratnam, P.: Changes in the velocity structure of the Greenland ice sheet, Science, 311, 986–990, https://doi.org/10.1126/science.1121381, 2006.

Schoof, C.: Ice sheet grounding line dynamics: Steady states, stability, and hysteresis, Journal of Geophysical Research, 112, F03S28+, https://doi.org/10.1029/2006jf000664, 2007.

Shepherd, A., Ivins, E. R., Geruo, A., Barletta, V. R., Bentley, M. J., Bettadpur, S., Briggs, K. H., Bromwich, D. H., Forsberg, R., Galin, N., Horwath, M., Jacobs, S., Joughin, I., King, M. A., Lenaerts, J. T. M., Li, J., Ligtenberg, S. R. M., Luckman, A., Luthcke, S. B., McMillan, M., Meister, R., Milne, G., Mouginot, J., Muir, A., Nicolas, J. P., Paden, J., Payne, A. J., Pritchard, H., Rignot, E., Rott, H., Sørensen, L. S., Scambos, T. A., Scheuchl, B., Schrama, E. J. O., Smith, B., Sundal, A. V., van Angelen, J. H., van de Berg, W. J., van den Broeke, M. R., Vaughan, D. G., Velicogna, I., Wahr, J., Whitehouse, P. L., Wingham, D. J., Yi, D., Young, D., and Zwally, H. J.: A Reconciled Estimate of Ice-Sheet Mass Balance, Science, 338, 1183–1189, https://doi.org/10.1126/science.1228102, 2012.

Straneo, F. and Heimbach, P.: North Atlantic warming and the retreat of Greenland's outlet glaciers, Nature, 504, 36–43, https://doi.org/10.1038/nature12854, 2013.

Straneo, F., Sutherland, D. A., Holland, D., Gladish, C., Hamilton, G. S., Johnson, H. L., Rignot, E., Xu, Y., and Koppes, M.: Characteristics of ocean waters reaching Greenland's glaciers, Annals of Glaciology, pp. 202–210, https://doi.org/10.3189/2012aog60a059, 2012.

Sutherland, D. A., Straneo, F., and Pickart, R. S.: Characteristics and dynamics of two major Greenland glacial fjords, Journal of Geophysical Research Oceans, 119, 3767–3791, https://doi.org/10.1002/2013jc009786, 2014.

Timmermans, M.-L.: Sea Surface Temperature [in Arctic Report Card 2016], http://www.arctic.noaa.gov/Report-Card, 2016.

Todd, J. and Christoffersen, P.: Are seasonal calving dynamics forced by buttressing from ice mélange or undercutting by melting? Outcomes from full-Stokes simulations of Store Glacier, West Greenland, The Cryosphere, 8, 2353–2365, https://doi.org/10.5194/tc-8-2353-2014, 2014.

van den Broeke, M. R., Enderlin, E. M., Howat, I. M., Kuipers Munneke, P., Noël, B. P. Y., van de Berg, W. J., van Meijgaard, E., and Wouters, B.: On the recent contribution of the Greenland ice sheet to sea level change, The Cryosphere, 10, 1933–1946, https://doi.org/10.5194/tc-10-1933-2016, 2016.

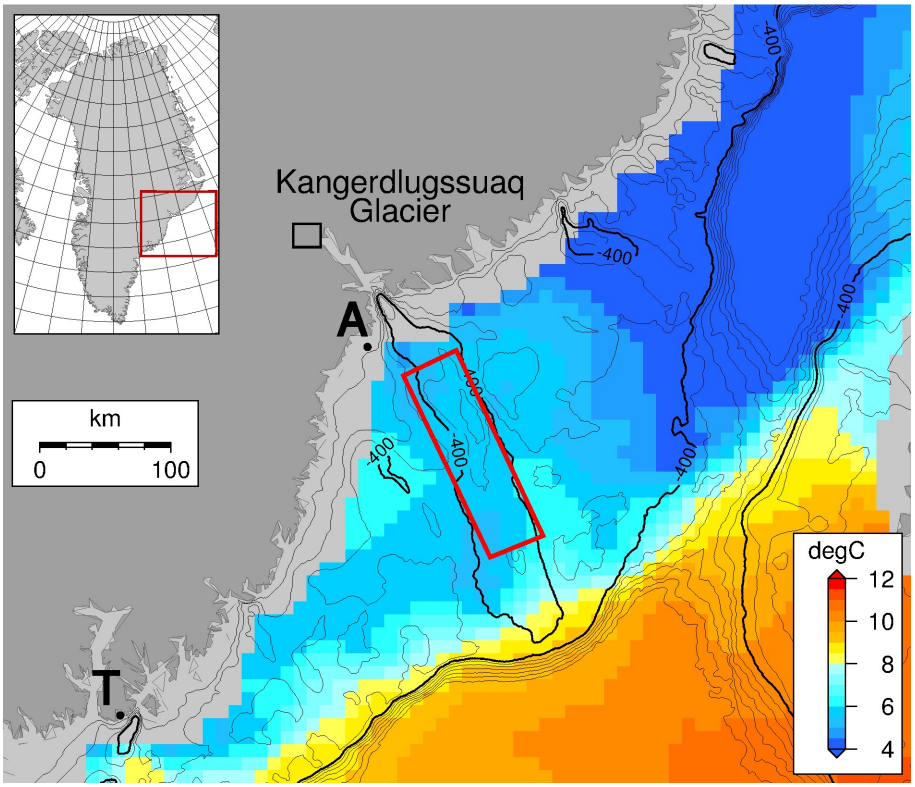

Figure 1. South-east Greenland with reanalysis 5 m ocean temperatures for July 2016. The bathymetric contours are in metres and are based on the International Bathymetric Chart of the Arctic Ocean Version 3 (Jakobsson et al., 2012). Small black box shows the Kangerdlugssuaq Glacier area covered by Fig. 7. Red box shows the area over which ocean temperatures were averaged for Figs 2 and 3. Aputiteeq and Tasiilaq weather stations are marked by the letters A and T, respectively.

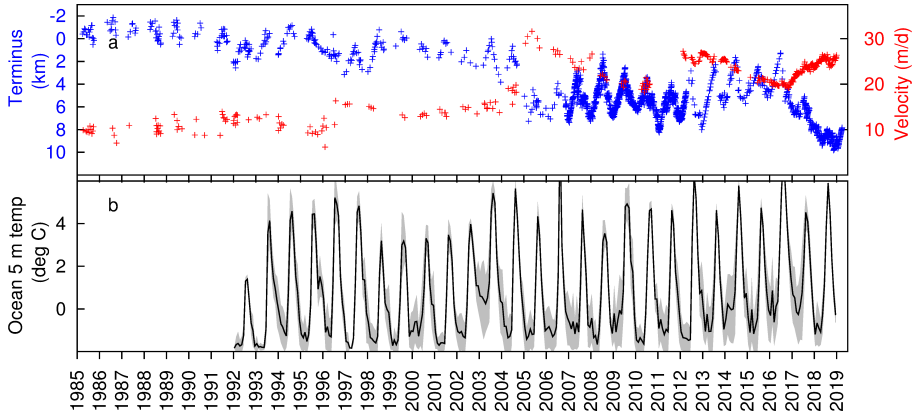

Figure 2. Time series of a) Kangerdlugssuaq Glacier front position and surface velocity. The y-axis distance scale for the front position matches the profile drawn in Fig. 7. Front positions and velocities are based on a variety of satellite images and the velocities were measured at the star marked in Fig. 7. Appendix Fig. A1 resolves which instruments contributed which observations. b) Kangerdlugssuaq trough monthly ocean potential temperature at 5 m averaged over the red box shown in Fig. 1. The grey shade shows ± one standard deviation around the mean.

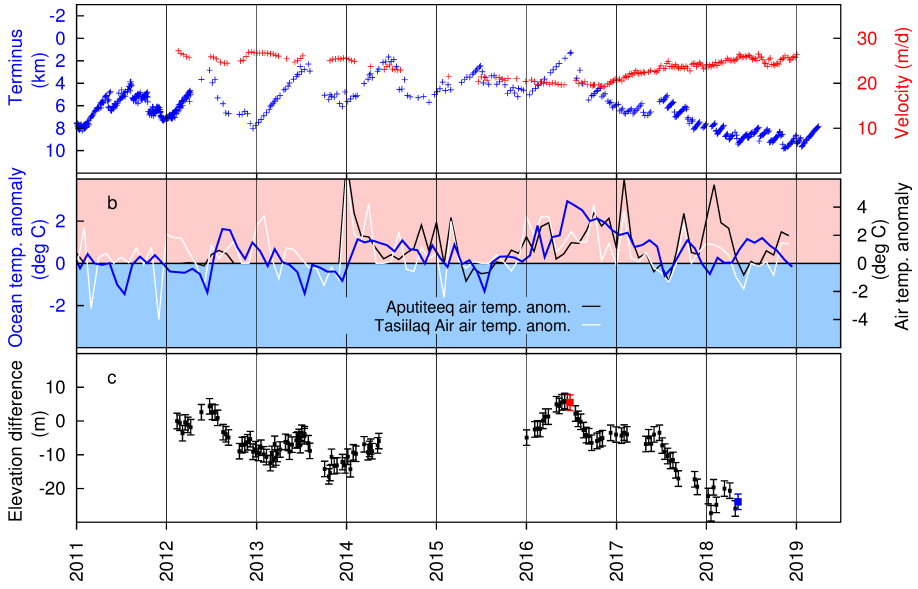

Figure 3. Time series plots. a) front position and surface velocity (note the change in front position and velocity scales compared with Fig. 2a). b) 2 m air temperature anomaly for Aputiteeq and Tasiilaq, and Kangerdlugssuaq trough ocean potential temperature anomaly at 5 m depth averaged over the red box shown in Fig. 1. c) Cross-glacier mean surface elevation difference taken from the TanDEM-X DEMs, the error bars represent the relative accuracy of ±2.3 m. The elevations are an average across the transect marked in Fig. 7, and the differences are relative to the first DEM.

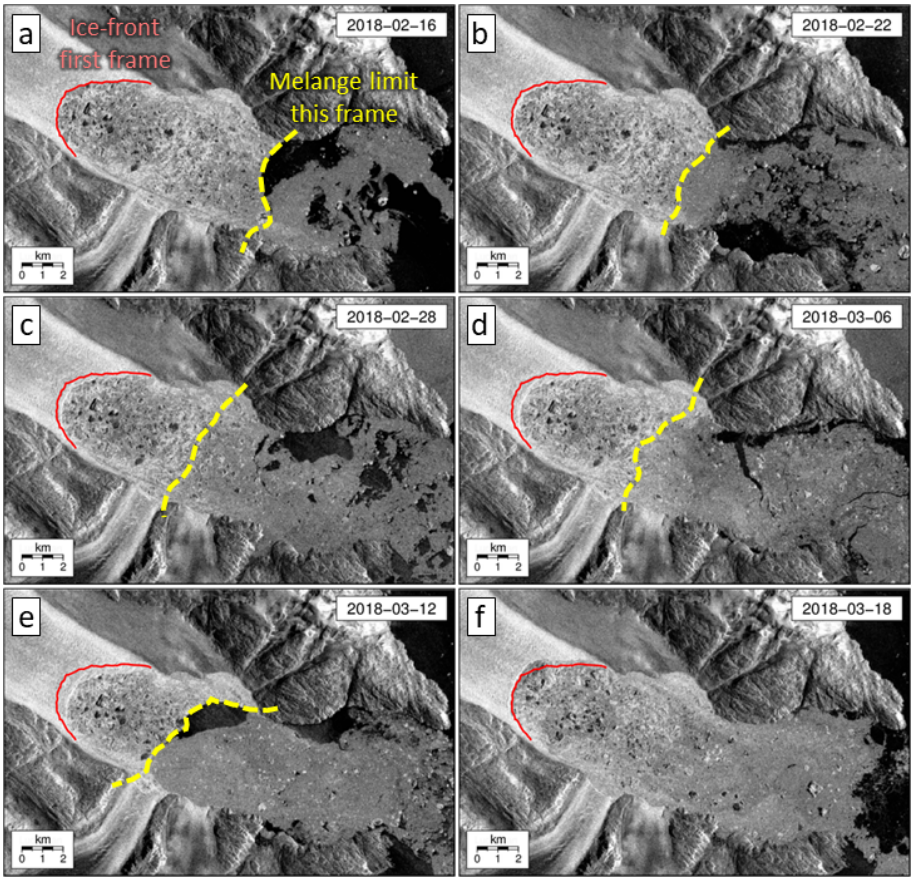

Figure 4. Sequence of Sentinel-1 SAR images of the Kangerdlugssuaq ice-front and fjord showing how the ice advances when mélange inhibits calving (panels a) to e)), then retreats again by calving because of loss or weakening of the mélange. The red line in each panel marks the ice-front position at the start of the sequence, and the yellow line marks the approximate extent of coherent mélange at each step. This behaviour is commonly seen in summer, but has recently also occurred in winter leading to ongoing glacier retreat.

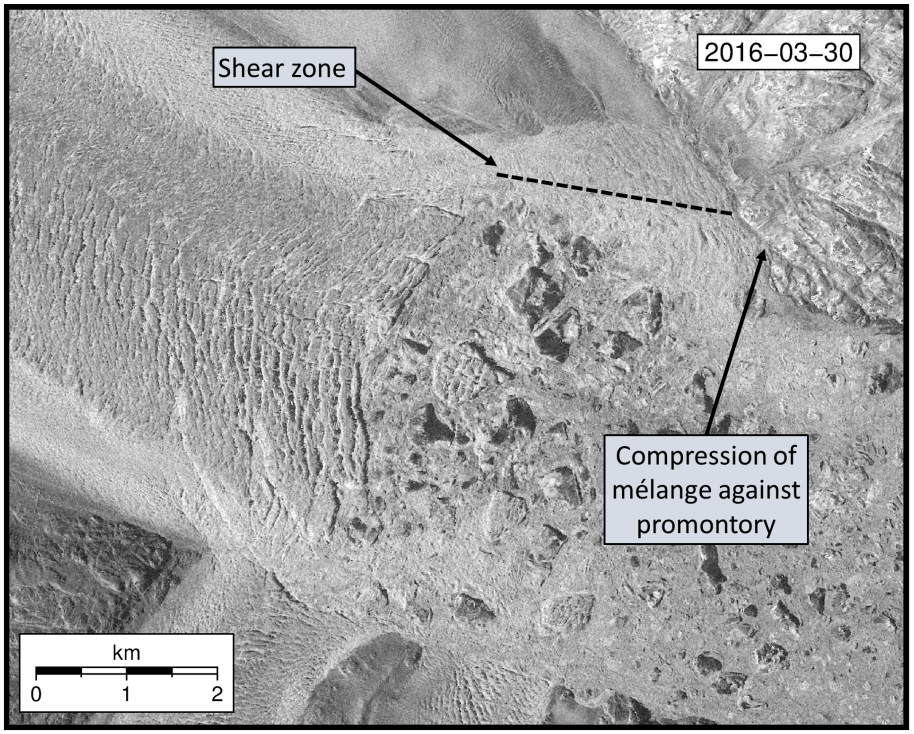

Figure 5. TerraSAR-X image showing the presence of ice mélange under compression, and the shear zone upstream of a promontory.

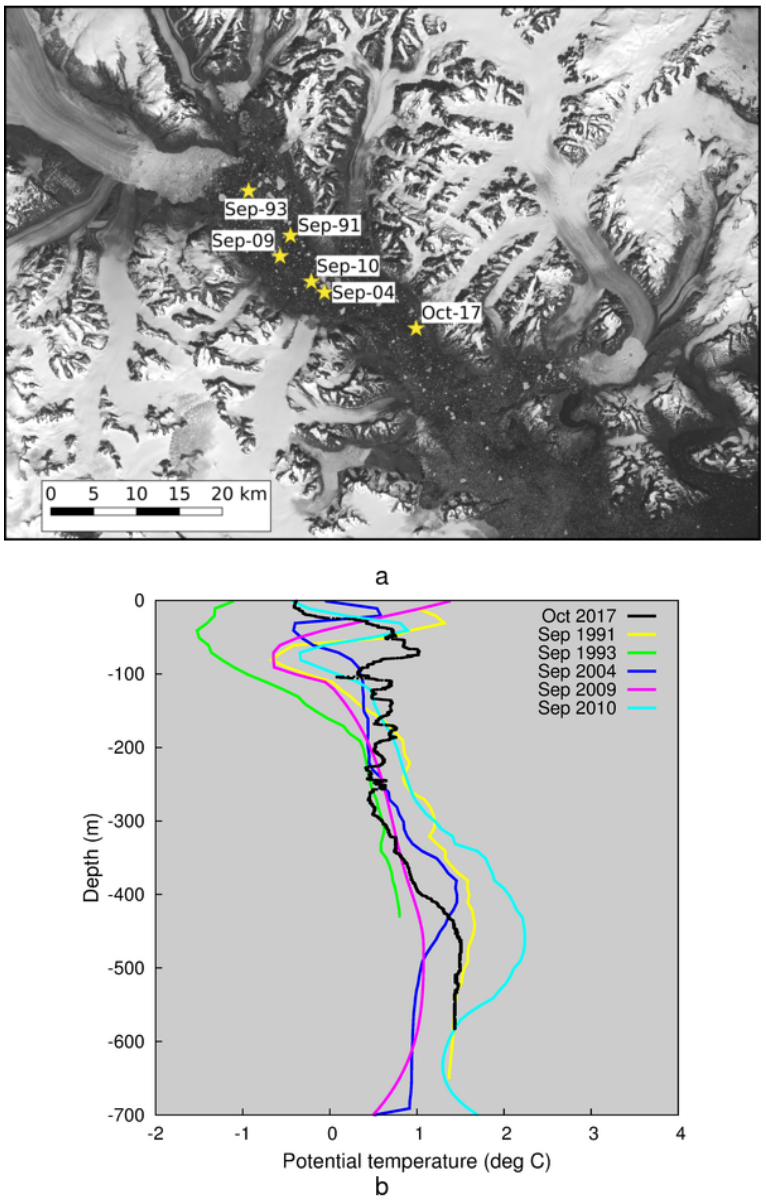

Figure 6. a) Location map (background Landsat Image 18/06/2016) and b) temperature profiles from published Conductivity Temperature Depth (CTD) data. September 1991 (Station K9, Andrews et al., 1994); September 1993 (Station KF3, Azetsu-Scott and Syvitski, 1999); September 2004 (Dowdeswell, 2004); September 2009 (Straneo et al., 2012); September 2010 (Inall et al., 2014); October 2017 (OMG Mission, 2016).

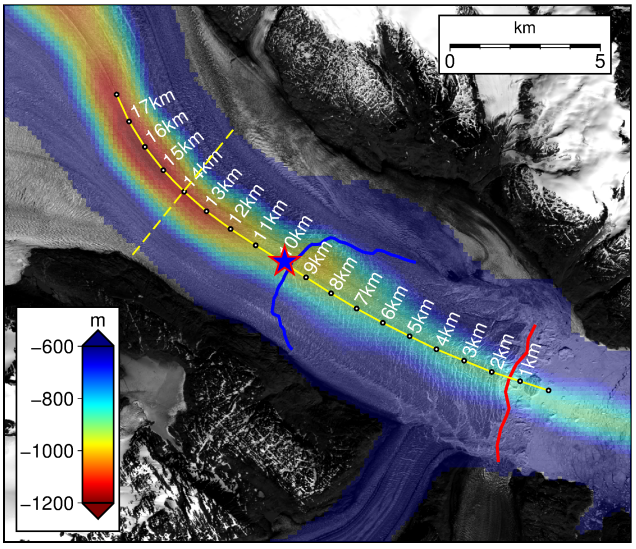

Figure 7. Glacier bed mapped using IceBridge BedMachine Greenland, Version 3 (Morlighem et al., 2017). The yellow profile and red and blue front positions relate to those drawn in Fig. 8. The dashed yellow transect indicates the line along which surface elevations were averaged for Fig. 3c. The star marks the velocity extraction location.

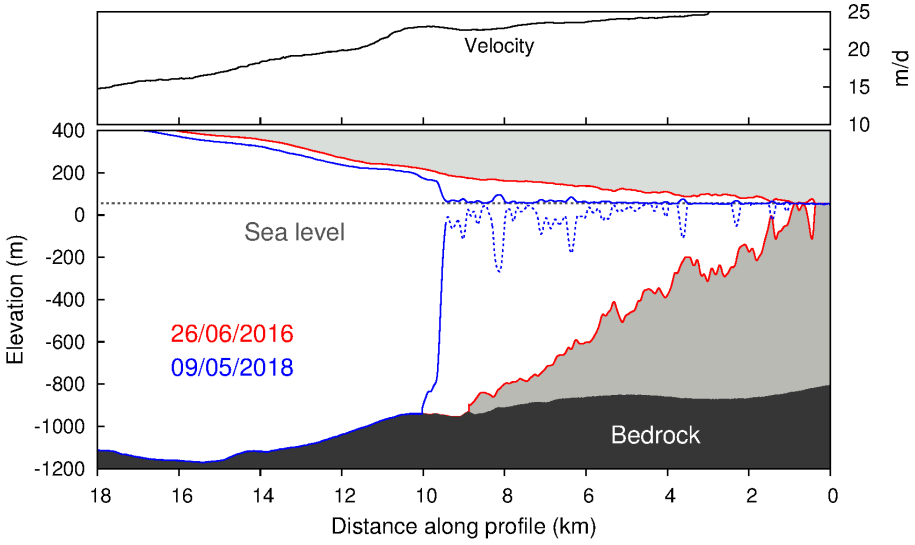

Figure 8. Surface elevation profiles for advanced and retreated front positions, corresponding to the same colour points plotted in Fig. 3c. The surface velocity profile is the result of feature tracking TanDEM-X data from 29/05/2014 to 09/06/2014

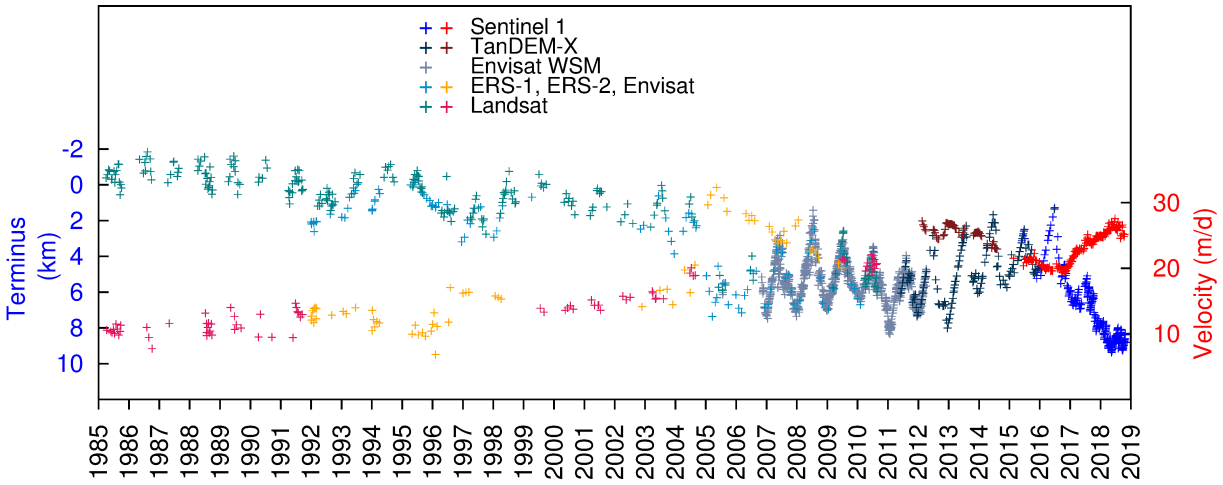

Figure A1. Time series of ice-front positions and velocity, with observations colour coded according to data source. Sentinel 1 includes 1A and 1B, TerraSAR-X refers to a single image from the TanDEM-X pair. Envisat WSM is Wideswath Mode data, European Remote Sensing satellites ERS-1 and ERS-2, and Envisat are Image Mode data, Landsat includes data from satellites 5, 7 and 8.

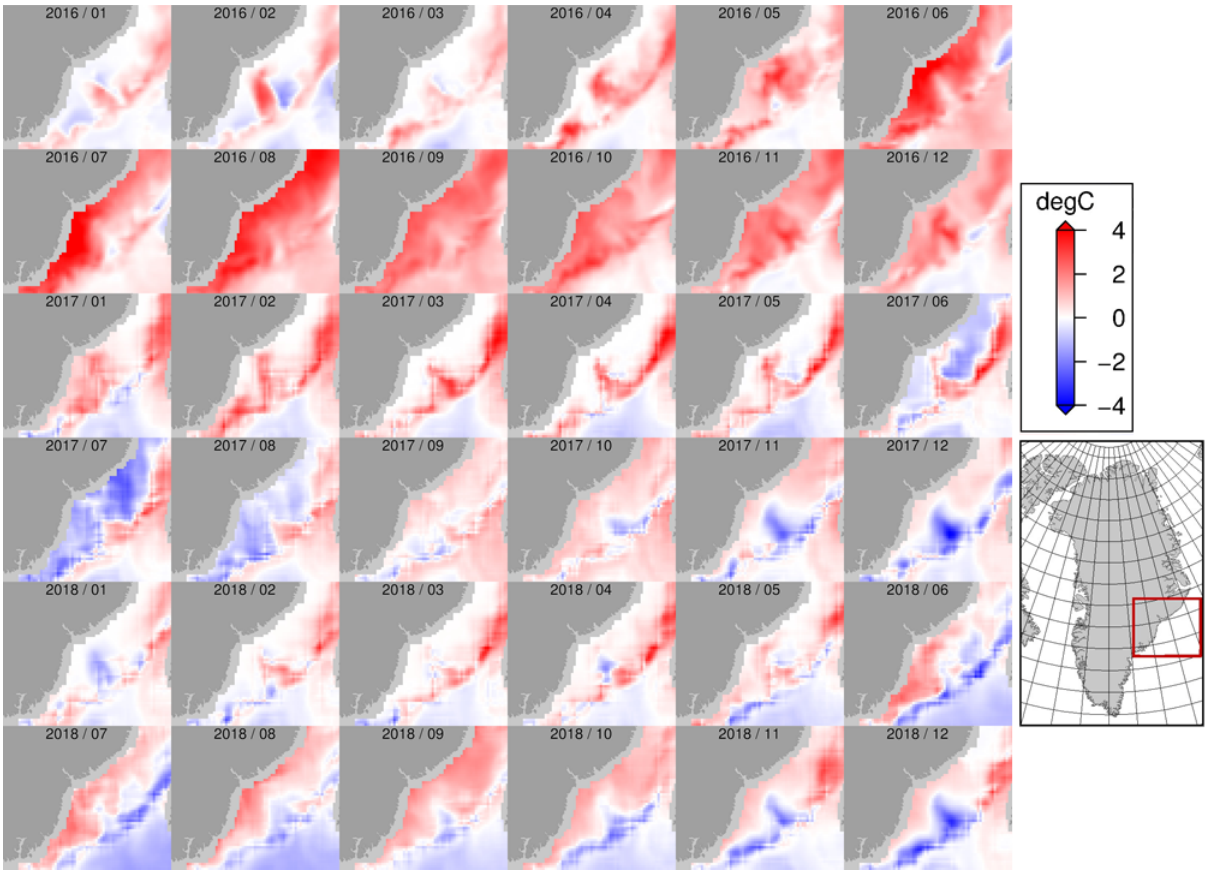

Figure A2. Anomalies in 5 m ocean potential temperatures. Temperatures for 1991–2017 are the Arctic Ocean Physics Reanalysis monthly mean data supplied by the Copernicus Marine Environment Monitoring Service (CMEMS). Temperatures for 2018 are based on monthly means of the Arctic Ocean Analysis and Forecast Product also from CMEMS. Anomalies are relative to the period 1992–2018.